SAND2019-8614B

Physics of Laser-Based Failure Analysis

Felix Beaudoin and *Edward Cole Jr,
Globalfoundries, East Fishkill, New York and *Sandia National Laboratories, Albuquerque, New Mexico
coleei@sandia.gov, phone 505-844-1421

Abstract

The basic physics behind active photon injection for local photocurrent generation and thermal laser heating are reviewed along with standard scanning optical microscopy failure analysis (FA) tools. The goals of the article are to arm analysts with an understanding of how the tools function and provide the tenants that will assist in determining how best to employ a given approach for a given situation. All of the methods described can be performed on a standard SOM (scanning optical microscope) using the proper laser wavelengths.

Introduction

Multiple scanning optical microscopy methods for integrated circuit (IC) FA have become essential tools to locate and diagnose defects and failure sites. The popularity of laser-based approaches stems from their relatively straight forward application, information delivered, and because of silicon's relative transparency to infrared wavelengths, applicability to backside FA.

Active laser-based approaches take advantage of direct IC interactions with focused, localized light. With illumination using shorter wavelengths/higher energies than the silicon indirect bandgap, the interactions are primarily photocurrent based using electron-hole pair production. Using longer wavelengths/lower energies than the silicon bandgap results in local heating of the target sample. While there are multiple stimulus variations and detection "schemes", the basics interactions of local leakage current generation and heating form the genesis of active laser FA. For both cases, understanding the interaction physics can be used for efficient FA.

This article will start by briefly reviewing the physics behind photocurrent generation in silicon and thermal laser stimulation (TLS). The discussion will include several models for understanding the local thermal effects on metallic lines, junctions, and complete devices. The article will conclude with a description and case study examples of multiple photocurrent and thermal injection techniques. The photocurrent examples are based on OBIC [1] and LIVA [2]. The thermal stimulus examples are OBIRCH/TIVA [3, 4] and SEI [4]. Lastly, we discuss the application of solid immersion lenses (SILs) to improve spatial resolution. Additional active stimulus methods incorporating electrical testing for detection, such as LADA and SDL are described in other chapters in this Desk Reference. Passive laser-based methods using reflected light variations through photo-electric interactions as well as passive light emission techniques are also explored in detail in their respective chapters.

Photocurrent Generation in Silicon

Active photon probing takes advantage of the interactions of a scanned photon beam with an IC. For photon energies greater than the indirect band gap of silicon ($\geq$1.1 ev or wavelength $\leq$ 1100 nm) electron-hole are generated pairs in silicon. Normally the electron-hole pairs will randomly recombine and there is essentially no net effect. However, when electron-hole pairs are generated near the interface between differently doped regions in an unbiased IC, the charge carriers are separated by the built-in potential between areas with different Fermi levels as shown in Figure 1. Biasing an IC alters the Fermi levels and hence alters the magnitude of electron-hole pair separation or photocurrent. In contrast to passive photon probing techniques, the detector in active photon probing is the IC itself. The relative transparency of silicon to near-infrared (NIR) wavelengths allows photocurrent generation from either side of the silicon, so the techniques can be applied for backside FA.

The photon beam source for active probing is usually a SOM, sometimes referred to as a laser scanning microscope (LSM). The basic SOM consists of a focused light spot that is scanned over the sample in a raster fashion. The light source is typically a laser. While dependent upon the particulars of the optics used, spot sizes on the order of 0.7X the laser wavelength used in air can be achieved and ~0.2X the wavelength achieved with an SIL (solid immersion lens). The spatial resolution of electrical effects on the device is limited by carrier diffusion lengths and carrier lifetimes, thermal conduction, device structure as well as spot size. By using different laser wavelengths and intensities, variations in the amount

of photocurrent can be obtained and backside photon probing performed.

Photocurrent generation near defects will alter the power demands of the test device and this can be used to localize structure and defects.

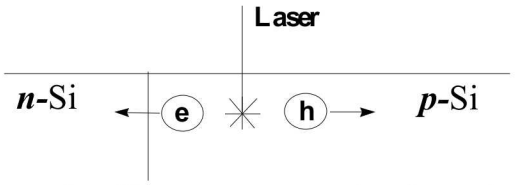

Figure 1. Photocurrent generation from photon produced electron hole pairs.

Thermal Gradient Generation and Physical Effects

TLS uses am NIR laser beam to thermally stimulate ICs. The laser energy is chosen below the silicon indirect bandgap energy (1.1eV) to avoid generation of photocurrents that could mask thermal effects [5]. As with photocurrent generation, the silicon substrate is relatively transparent at NIR wavelengths. Laser beam absorption depends on the doping type and level [6,7], but in general TLS is applicable to front and backside FA. For heavily-doped silicon substrates, the die backside may be thinned (e.g. 100µm) to minimize laser power losses due to absorption for thermal or photocurrent analyses [8,9].

A small portion of the absorbed NIR laser beam principally heats IC metallic elements, and to a lesser extent, polysilicon elements and highly doped substrate areas. It modifies the electrical properties of the heated medium, namely its resistivity. This change of resistivity alters applied current (or voltage). These electrical changes inside the device may be monitored at the power supply nodes. Correlating IC power consumption changes with the laser spot location provides precise localization of thermally sensitive areas such as resistive defects.

TLS induced IC power consumption variations can be classified as follows:

i) resistance variation (OBIRCH, TIVA)
ii) thermoelectric energy conversion or Seebeck effect (SEI)

Resistance variation

A temperature increase in the heated elements induces a resistivity variation, modeled as follows:

$$\Delta\rho = \rho_0 \alpha_{TCR}(T-T_0) \quad (1)$$

where ρ_0 is the resistivity, α_{TCR} is the thermal coefficient of resistance, and ΔT is the temperature variation.

When the IC is biased, the thermally induced resistance variation is monitored through the device voltage or current consumption depending on the biasing method. This is illustrated by the following equations:

$$\Delta V = \Delta R_{IC} I_S \quad (2)$$

$$\Delta I = -\left(\Delta R_{IC} / R_{IC}^2\right) V_S \quad (3)$$

where ΔR_{IC} is the resistance variation and R_{IC} is the IC resistance, I_S is the current source and V_S the voltage source.

Seebeck effect

The Seebeck effect is based on the generation of an electromotive force by temperature gradients at junctions composed of two different materials (e.g. aluminum-tungsten) [10]. The Seebeck voltage induced when one side of a thermocouple is heated is given by:

$$\Delta V = (Q_1 - Q_2)\Delta T = Q_{1-2}\Delta T \quad (4)$$

where Q_1, Q_2 are the respective thermoelectric power of materials and Q_{1-2} the relative thermoelectric power difference of the two materials.

When no bias is applied to the IC, the measured voltage variation is directly related to the Seebeck effect. This effect is also present when the IC is biased, but its contribution is often negligible compared to the TLS signal due to the resistance variation and transistor amplification [4].

Thermal Models

We present several models aimed at understanding the TLS signal when the NIR laser beam is scanned over a single metallic line.

Thermal simulation model

To gain insight into the heating dynamics, a 3D finite element model of a 1µmx0.5µm aluminum line embedded in silicon dioxide was studied. A schematic

diagram of the modeled structure is shown in Figure 2. The material properties of thin film Al, bulk SiO_2 and Si, given in Table 1, were assumed to be temperature independent. A detailed description of the model is given in [11].

The TLS effect was dynamically modeled for the two following cases:

(1) Longitudinal case when the laser beam is scanned perpendicular to the metal line.
(2) Transversal case when the laser beam is scanned parallel to the metal line.

Thermal simulations were performed for a laser beam power of 100mW, a laser beam radius of 0.65µm and an initial temperature of 25°C. Both transversal and longitudinal cases were resolved for a fast scanning speed of 1.23m/s and slow scanning speed of 0.00768m/s. These respectively correspond to a 1024x1024 frame scanning time of 2s when a 5x objective is used and to a scanning time of 16s when an objective of 100x is used.

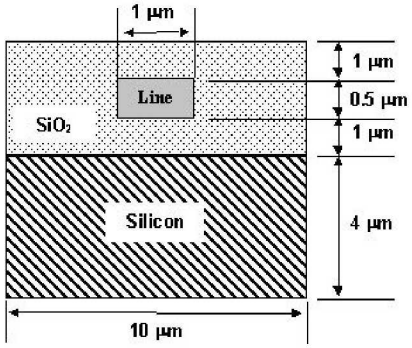

Figure 2. Schematic diagram of the modeled structure.

The model confirmed that the metal line reaches the permanent regime at the slowest scanning speed. The temperature profile for the longitudinal case is shown in Figure 3. The peak temperature is obtained in less than 10µs.

The temperature profile along the metal line at the hottest spot for all cases is given in Figure 4. A permanent regime temperature of 79.9°C was obtained. However, this maximum temperature was not reached for the fastest scanning speed. At low magnification, defects may be undetected if the scanning speed is not sufficiently slow. For instance, a 1024x1024 frame scanning time higher than 4s is required when a 5x objective is used.

Table 1: Structural parameters [12,13,14].

	Al	**SiO_2**	**Si**
Density (U) (Kg/m^3)	2702	2190	2330
Specific heat (c) ($J\ Kg^{-1}\ K^{-1}$)	896	1400	703
Conductivity (K) ($W\ m_{-1}\ K_{-1}$)	246	1.4	141
Absorption coefficient (D) (cm^{-1})	$1.3x10^6$	0	NA
Reflectivity (R) @ 1.3 Pm	97%	0	NA

.

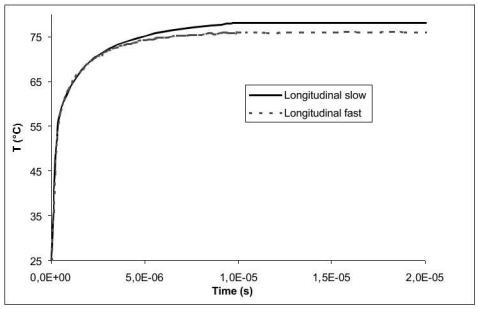

Figure 3. Temperature profile as a function of time for the longitudinal case at both scanning speeds.

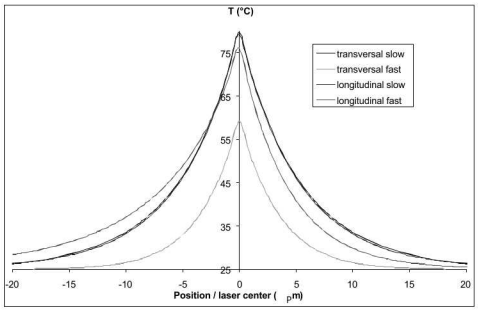

Figure 4. Temperature profile along the metal line for all the considered cases. Absolute temperature values are calculated for a 100 mW laser power.

Simulations calculated a thermal spreading limited to approximately 30 µm and a separation of less than 0.1µm between the hottest spot and the laser beam.

Finally, it was found that the temperature increases linearly with the laser power. Given sufficient time for the permanent regime to be established, the peak temperature variation induced by laser heating in a 1µm x 0.5µm aluminum line is:

$$\Delta T_{max} = 0.55\,^{o}C/mW \quad (5)$$

Resistance variation

Resistance variation of the aluminum was calculated in the permanent regime. Resistance change, ΔR, can be calculated from the average temperature along the metal line at a given time ($T_{avg}(t)$) according to the following analytical model:

$$\Delta R(t) = \rho_0 \alpha_{TCR} (L/S)(T_{avg}(t) - T_0) \quad (6)$$

where ρ_0 is the metal resistivity, α_{TCR} is the metal temperature coefficient of resistance, L the length of the line, S its cross-section and T_0 the initial temperature.

Equation 6 points out the inversely proportional relationship of the resistance change to the metal line section. The resistance change of smaller elements is favored compared to larger ones.

In the case of the 1µmx0.5µm aluminum line, maximum resistance change in the permanent regime is given by:

$$\Delta R_{max} = 1.7x10^{-3}\,\Omega/mW \quad (7)$$

This calculation was done using a resistivity (ρ_0) of $4.8x10^{-6}\Omega cm$ and a temperature coefficient of resistance (α_{TCR}) of $3x10^{-3}K^{-1}$. These values are typical of an Al technology CMOS IC process [15].

The voltage or current variations due to the resistance variation are calculated with equations 2 or 3. The reduction or increase in the power consumption variation is directly related to the metal temperature coefficient of resistance. Therefore, the polarity of the TLS signal provides direct information on the resistive defect nature. For an aluminum line submitted to a constant current, a voltage increase is expected. This is not the case for polysilicon as its temperature coefficient of resistance depends on its nature such as its doping level.

Electromotive force generation

The Seebeck voltage induced at an interface such as that shown in Figure 5 can be calculated from equations 4 and 5. The Seebeck coefficients for different materials are given in Table 2.

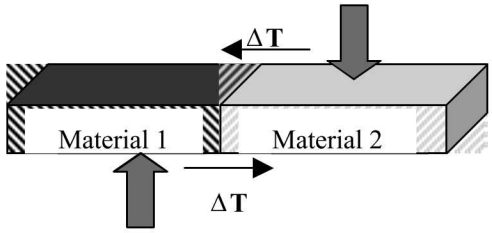

Figure 5. Thermal gradients induced at a thermocouple as a function of the laser beam position.

The polarity of the Seebeck voltage depends on the laser beam position relative to the junction. For example, when the laser beam crosses the junction, the polarity of the Seebeck voltage is inverted since the induced temperature gradient is in the opposite direction.

Table2. Seebeck coefficients for different materials [12,16].

	Q (PV/°C)
Al	-3.4*
W	3.6*
Al / n+ Si	287**
Al / p+ Si	-202**

**measured relative to copper*

***relative thermoelectric power for a 10^{18} cm^{-3} doping.*

Upon TLS, the temperature can be uniformly distributed throughout the whole volume of the two materials composing the junction due to heat spreading. This thermal spreading can attenuate the Seebeck voltage. However, an interface defect such as a hole can create an imbalance between the two opposite Seebeck voltages, therefore allowing its localization.

The Seebeck effect is best observed when no bias is applied to the IC. Indeed, the power generation variations are generally small compared to induced resistance variations. Another advantage of non-biased TLS is the very small electrical power involved, which is in the order of pico-watts. Defects, as well as the device under test, are therefore unaltered, which can be very important for later physical analysis.

IC effect model

In complex ICs, the TLS signal also depends on the IC's response to the resistance variation and/or the induced electromotive force. The IC effect was simulated with Spice for a resistive defect short-circuiting the PMOS of a CMOS inverter as shown in Figure 6. TLS of the resistive defect was simulated by varying the resistance value.

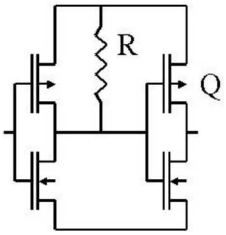

Figure 6. CMOS inverter modeled in SPICE.

The total current variation as a function of the resistance change is plotted in Figure 7.

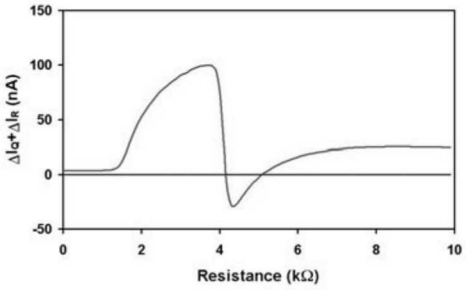

Figure 7. Total current variations in the CMOS inverter shown in Figure 7.

The magnitude and sign of the current variation strongly depend on the resistance value. The physical model predicts a current decrease upon a resistance increase when a voltage bias is applied to the CMOS inverter. This is the case only for a small range of resistance values.

Transistor heating model

The FET transistors are also affected upon TLS. This is understood through the current-voltage characteristics of an idealized MOSFET in the saturated region [17]:

$$I_{Dsat} \cong \frac{Z\mu\varepsilon_{ox}}{2dL}\left(V_G - V_T\right)^2 \tag{8}$$

where Z and L are respectively the channel width and length, d is the thin oxide thickness, μ is the mobility, ε_{ox} is the oxide dielectric constant, V_G is the gate voltage and V_T is the threshold voltage.

A temperature increase in the channel results in a mobility change as well as a voltage threshold change [18].

The channel region of the FET is not directly heated by the laser beam, but rather indirectly through heat diffusion from neighboring regions as indicated in Figure 8. The FET device regions efficient in converting NIR light into heat are:

- Heavily doped regions such as source and drain
- Polysilicon gates
- Buried layers

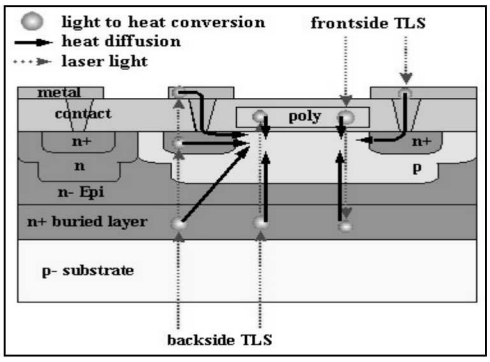

Figure 8. Light transmission and heat diffusion for front-side and backside TLS.

Oversize FET test structures were studied to understand their behavior under TLS. These devices, built in a BiCMOS technology, are characterized by a 10x10Pm^2 gate area and a 15nm gate oxide. The TLS results obtained from the front and backside of the FET when biased in the saturated region are presented in Figure 9. A high TLS signal is observed at the gate level due to indirect heating of the channel by heat diffusion though the thin gate oxide. The source and drain region as well as the interconnects were also found to affect the drain current. The higher thermal efficiency obtained from the backside can be attributed to heat generation at the buried layer.

Finally, the maximum current change was measured for different drain to source voltages under TLS. As can be seen in Figure 10, the output characteristics indicate a current change proportional to the FET drain current. Therefore, the TLS method is able to localize conducting FET transistors. The magnitude of the TLS signal depends on the biasing condition of the FET.

The TLS signal is not always directly interpretable in complex ICs. The magnitude and polarity of the TLS signal is strongly influenced by the location and the value of the resistive defect. In addition, junctions as well as conducting FETs may be visualized in the TLS image.

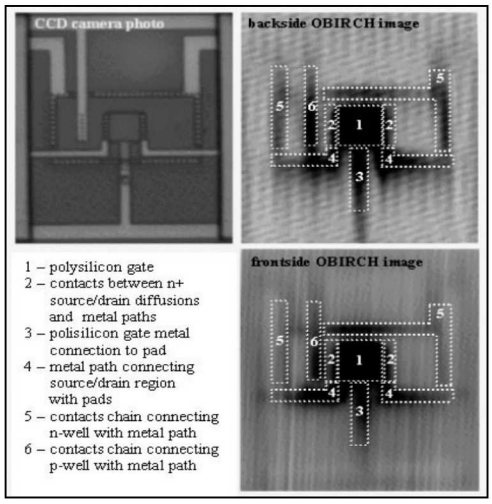

Figure 9. Front side and backside TLS images obtained on oversized FET test structures.

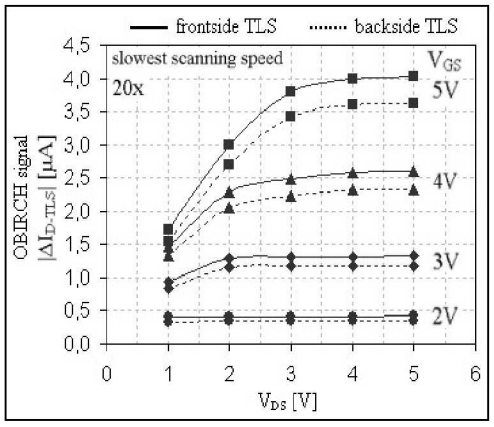

Figure 10. Front side and backside TLS induced current variation as a function of VDS for various values of VGS.

The knowledge gained from the TLS models is manifold. The TLS method:

- Is relatively fast. The thermal permanent regime is reached in less than 10μs.
- Can precisely localize current paths and defects. The hottest temperature occurs at the laser spot center.
- Is applicable to metallic, polysilicon and highly doped silicon structures.
- Is efficient in localizing short-circuit type defects when charge flows through them. The resistance variation of smaller elements is higher than for larger ones.
- Provides information on the nature of the material. The polarity of the TLS signal depends on the polarity of the temperature coefficient of resistance.
- Allows the localization of material discontinuities, which can be defect induced, through the Seebeck effect.
- Can detect and localize conducting FET transistors.

Furthermore, the high number of metal levels used in today's ICs can result in the delocalization of the thermally sensitive area relative to the resistive defect location. This is the case if the resistive defect is not directly heated by the laser beam (e.g. due to metallization masking), but through heat diffusion from the nearest heated structure.

Detection Techniques and Setups

The photocurrent and TLS methods are usually implemented on commercial visible and NIR laser-scanning microscopes. The laser wavelength is typically 532 nm and 1064 for photocurrent generation and 1300nm or 1340nm for thermal stimulus with laser powers up to 500mW.

Systems also integrate the following elements:

i) Voltage or current source to bias the IC.
ii) Low noise amplification scheme to amplify small power consumption variations.
iii) Laser scanning synchronization system to synchronize the laser beam position with power consumption variations.
iv) Imaging software to visualize power consumption variations overlaid on the IC image.

One of the key system components is the amplification scheme used to pick up the extremely small voltage or current variations caused by laser stimulus. Commercial systems are available, but specifically designed amplifiers have a bandwidth adaptable to the laser scanning speed with high adjustable gain.

Several techniques have been developed and appropriately named to reflect their novelty. They are presented in Table 3. The difference between them lies in device biasing and signal detection schemes.

The CC-OBIRCH (Constant Current Optical Beam Induced Resistance Change), LIVA (Light-Induced Voltage Alteration) and TIVA (Thermally-Induced Voltage Alteration) techniques use a constant current source with a voltage amplifier mounted in parallel to the IC. The same setup, with or without the current

source, can be used for the SEI (Seebeck Effect Imaging) technique.

Table 3: TLS techniques

TLS techniques	Source	Amplifier
CC-OBIRCH [3] TIVA/SEI [4] LIVA [2]	Current	Voltage
OBIRCH [19] IR-OBIRCH [5]	Voltage	Current
TBIP [20] XIVA [21]	Voltage	Voltage
SEI [4] OBIC [1]	Current or no bias	Voltage

For the OBIRCH (Optical Beam Induced Resistance Change) and IR-OBIRCH (Infrared Optical Beam Induced Resistance Change) techniques, a constant voltage source is used. A current amplifier is mounted in series with the IC. For OBIC (Optical Beam-Induced Current) a zero bias voltage source is typically used.

In the TBIP (Thermal Beam Induced Phenomenon) and XIVA (Externally Induced Voltage Alterations) techniques, the current amplifier used in the OBIRCH configuration is replaced with a specific amplification scheme composed essentially of an inductor and a voltage amplifier.

The sensitivity of the TLS or OBIC/LIVA methods strongly depends on the noise related to both the biasing and detection scheme. The biasing source should be as noise free as possible. The constant current or constant voltage source noise detected by the amplifier is more or less significant depending on the IC resistance or photocurrent induced signal strength. For failed ICs characterized by a high resistance, it is more appropriate to use a voltage source. For low resistance leakage paths, the use of a current source may reduce the noise associated with the biasing scheme. The sensitivity can also be improved by using a lock-in detection scheme. This option is proposed on some commercial TLS tools.

Laser-Based Technique Case Studies

The following examples demonstrate how the two physical effects discussed above, localized photocurrent generation and thermal stimulus, can be in FA.

OBIC (Optical Beam-Induced Current)
In OBIC, photocurrents are used directly to produce an image of Fermi level variations across an IC [1]. For typical operating conditions (front side examination with a 633 nm, 5 mW HeNe laser), the peak OBIC currents on an unbiased IC are on the order of tens of microamperes. The OBIC setup is shown schematically in Figure 11. Changes in the amount of electron-hole pair recombination current produce the contrast in an OBIC image. The resulting image displays the locations of buried diffusions on the sample as shown in Figure 12. In addition to junction location, variations in photocurrent can also result from defects associated with the junction such open interconnections, silicon crystal defects, and overstress damage. Any damage that alters the local Fermi levels on the IC will alter the amount of photocurrent produced. Some semiconductor parameters such as minority carrier lifetimes, diffusion lengths, and surface recombination velocity can be determined by OBIC and the electron beam analog EBIC [22].

Electrical accessibility to the photocurrent generating site and interpretation of the OBIC signal limit the use of OBIC on ICs. Abnormal photocurrent production may be undetected if they are not readily observable via the IC's external interconnections. Electrical biasing can improve the observability of internal IC nodes, but large IC background currents can overwhelm the OBIC signals making them difficult to detect. Once acquired the OBIC signals of "good" vs "bad" ICs can be difficult to interpret, usually requiring a detailed knowledge of the IC design and comparison with a non-defective sample.

Photocurrent generation requires that photons reach the junctions of interest. Since metallization is opaque, signals cannot be obtained in areas covered by metal. Backside examination of ICs has been well established and takes advantage of silicon's relative transparency to photons with energies just above the indirect silicon bandgap energy (Figure 13) [23]. Generation of OBIC signals from backside IR illumination requires that the photon wavelength be long enough to penetrate through the silicon substrate but short enough (have enough energy) to produce electron-hole pairs in the junction regions.

OBIC and the other laser-based techniques can demonstrate improved signal sensitivity using a pulsed laser and lock-in technology. This may offer other

improvements as instrumentation and laser pulsing capabilities advance.

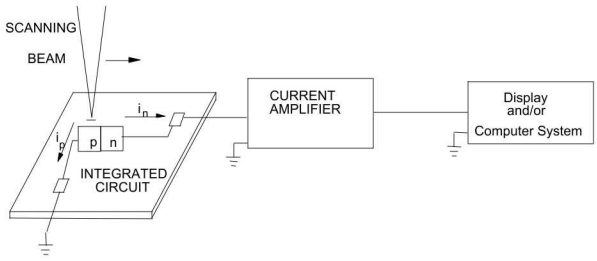

Figure 11. OBIC setup.

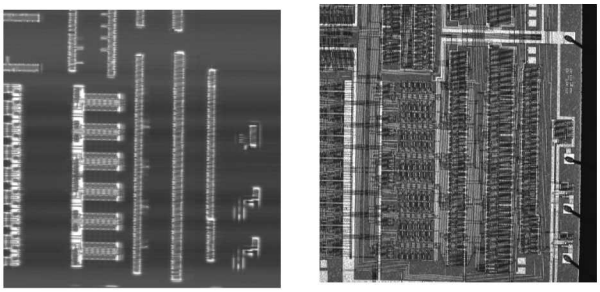

Figure 12. An OBIC image (left) showing the position of diffusions on an IC. A reflected light image (right) is shown for registration.

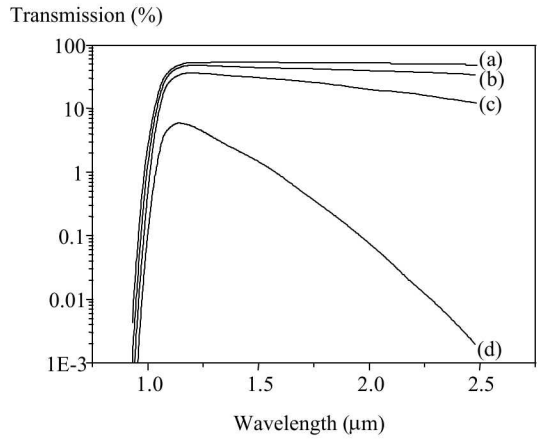

Figure 13. Percent transmission of light through 625 μm of p-doped silicon having doping concentrations of (a) $1.5x10^{16}$, (b) $3.3x10^{17}$, (c) $1.2x10^{18}$, and (d) $7.3x10^{18}$ cm^{-3}.

Light-Induced Voltage Alteration (LIVA)

LIVA [2] is a Scanning Optical Microscopy (SOM) technique developed to localize diffusions associated with IC defects. The high selectivity of LIVA permits examination of the entire IC die in a single, unprocessed image. LIVA examination of an IC's surface from the front side is performed using a visible laser light source. By using an infrared light source LIVA has shown applicability to backside examination of ICs.

LIVA, like OBIC, takes advantage of photon generated electron-hole pairs to yield IC functional and defect information. The device under examination is biased using a constant current power supply. LIVA images are produced by monitoring the voltage shifts in the power supply as the optical beam from the SOM is scanned across the device. Voltage shifts occur when the recombination current increases or decreases the power demands of the IC.

The LIVA measurement and imaging of voltage shifts rather than directly observing the photo-currents has two advantages. First, the IC will act as its own amplifier producing a much larger LIVA voltage signal than a photo-current signal. This is in part due to the difference in "scale" for voltage and current on ICs. For example, a CMOS IC biased at 5V had a photo-current increase of 100 nA (from 90 nA to 190 nA) when a transistor gate was exposed to the SOM beam. When the same conditions were repeated for the IC biased with a constant current supply set to yield 5V with no illumination (90 nA supplied), the voltage decreased by 2.4 volts (from 5 V to 2.6 V). A second advantage is that IC voltages are much simpler to measure than IC currents. Current measurement is in series, with the measurement system becoming "part" of the IC. Because of this series measurement, most current amplification systems will have maximum current limits (typically 250 mA) that limit the operational range without modifications. There is also the added complication of sometimes needing to measure a relatively small photo-current against a large dc background current. Voltage measurements are made in parallel and are therefore "separate" from the IC with none of the current measurement limitations. Small changes in voltage are easily measured using an ac coupled amplifier immune to background dc voltages. This relative signal difference and simpler equipment setup make LIVA far more attractive than conventional photo-current methods.

Defects on ICs, such as diffusions connected to open conductors and electrostatic discharge damage, produce relatively large LIVA signals when compared to the LIVA signal of biased diffusions under similar conditions (10 to 1000 or more times greater). This relative difference is used to produce highly selective LIVA images for defect localization.

Backside LIVA examination is performed using a NIR source. The source wavelength must be large enough

to take advantage of silicon's greater transparency to infra-red light, but small enough to generate electron-hole pairs in the diffusion regions of the IC.

Figure 14 displays how a defect can be localized using LIVA from the backside of an IC. The IC is a radiation hardened version of the Intel 80C51 microcontroller. A 5 mW, 1152 nm laser was used to acquire the images. The LIVA image in Figure 14a displays a small signal in the lower right. Figure 14b is a reflected light image showing the same field of view. Note that the entire IC is being examined in this field of view. Figures 14c and 14d are higher magnification LIVA and reflected light images of the area identified in Figures 14a and 14b. Later analysis indicated that the LIVA signal is caused by an open metal-1 to silicon contact. Note that the open contact area is completely covered by a metal-2 power bus that would obscure any front side examination.

Optical Beam Induced Resistance Change (OBIRCH), Thermally-Induced Voltage Alteration (TIVA) and Seebeck Effect Imaging (SEI)

OBIRCH [3], TIVA and SEI [4] are different variants of a Scanning Optical Microscopy (SOM) technique developed to localize opens (SEI) and short circuits (OBIRCH/TIVA) on ICs with localized heating. The high selectivity of both variants permit examination of the entire IC die in a single, unprocessed image. At the wavelengths used localized heating can be produced from the front or backside of the IC making defect localization possible from either side.

As discussed above, OBRICH, TIVA, and SEI are TLS approaches that use a NIR wavelength longer than 1.1 μm (the indirect bandgap in silicon) to produce localized heating on an IC without electron-hole pair production. In OBIRCH and TIVA, the localized heating changes the resistance of a short site.

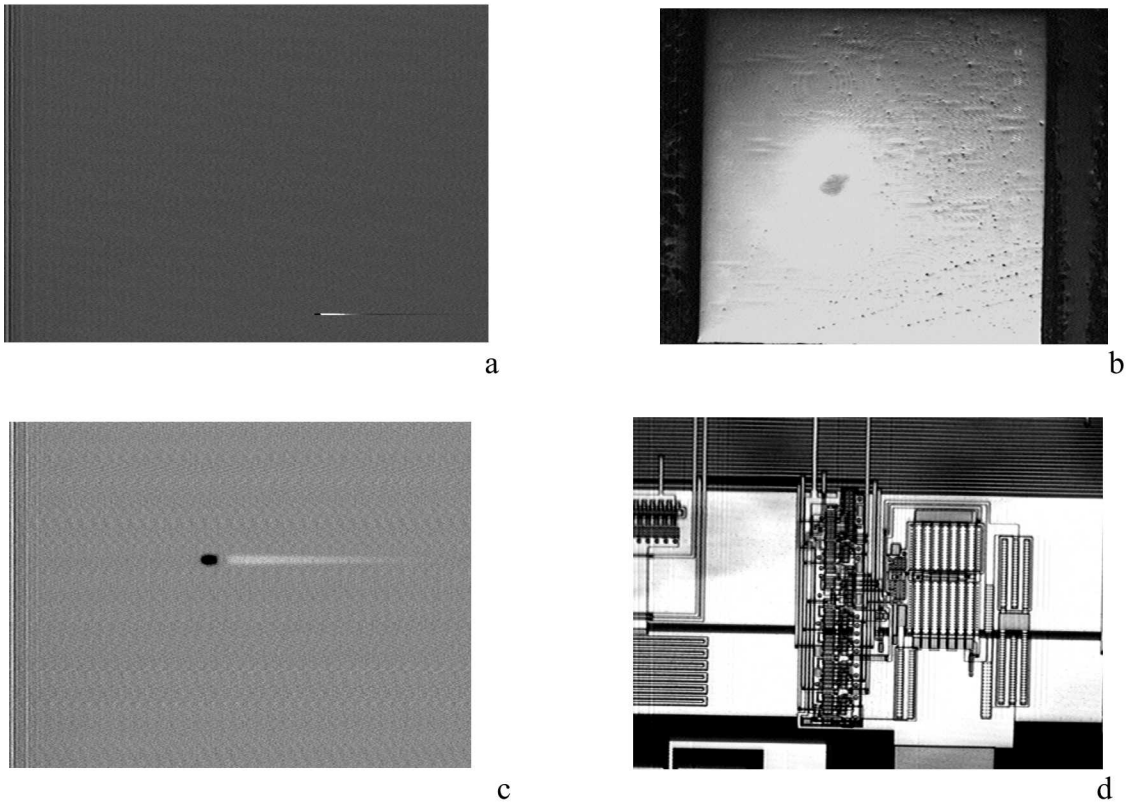

Figure 14. Backside LIVA examination of a microcontroller: LIVA image (a) indicating the area of an open metal-1 to silicon contact, backside reflected image (b) showing the same field of view as Figure 14a, higher magnification LIVA image (c) of the defect in Figure 14a, and a reflected light image (d) of the same field of view as Figure 14c. The defect site is completely covered by a metal-2 power bus from the IC's front side.

If the short site is a conductor, the resistance will increase with temperature. If the short site is a semiconductor, the resistance will decrease with increasing temperature. In any event the resistance of the short site changes with temperature. As the resistance of the short site changes the power demand of the IC changes, assuming the short site has a voltage gradient across it. This effect of localized heating on IC short circuits and the subsequent IC power demand changes was first shown in the OBIRCH (optical beam induced resistance change) technique. TIVA displays an increase in detection sensitivity using the constant current biasing approach applied in LIVA. Figure 15a displays an entire 1MB SRAM with a short site as indicated by the TIVA image. Note that the short site has been localized in a single image. Figure 15b is a reflected light image of the same field of view for registration. Figure 16 is a backside TIVA/reflected light image pair of a short site. The particle producing the short cannot be seen in Figure 16b because it is on top of the shorted metal-1 interconnections. The example in Figure 16 demonstrates how heat can travel through a metal layer to detect a defect where photons cannot.

Localized heating can also be used to locate open conductor sites from the front and backside of an IC. Open conductor sites are identified through the use of the Seebeck effect. As shown above, thermal gradients in conductors generate electrical potential gradients with typical values on the order of mV/K. This is known as thermoelectric power or the Seebeck Effect and refers to the work of Thomas Johann Seebeck (1770-1831). The most common application of thermoelectric power is the thermocouple, which uses the difference in thermoelectric voltages of two different metals to measure temperature. If an IC conductor is electrically intact and has no opens, the potential gradient produced by localized heating is readily compensated for by the transistor or power bus electrically driving the conductor and essentially no signal is produced. However, if the conductor is electrically isolated from a driving transistor or power bus, the Seebeck Effect will change the potential of the conductor. This change in conductor potential will change the bias condition of transistors whose gates are connected to the electrically open conductor, changing the transistors' saturation condition and power dissipation. An image of the changing IC power demands (via constant current biasing) displays the location of electrically floating conductors. For the laser and SOMs used to date a maximum temperature gradient of about 30 ^{o}C has been achieved, with most work producing temperature changes of 10 ^{o}C or less. The resulting small changes in open conductor potential need the sensitive constant current biasing approach for defect detection. Figure 17a shows a backside SEI image of a FIB-opened conductor. Figure 17b is a reflected light image for registration. The open conductor can be seen as well as strong contrast at the metal-polysilicon interconnections. The enhanced contrast is believed to result from the thermopower difference in the two different materials (polysilicon and the metal conductor).

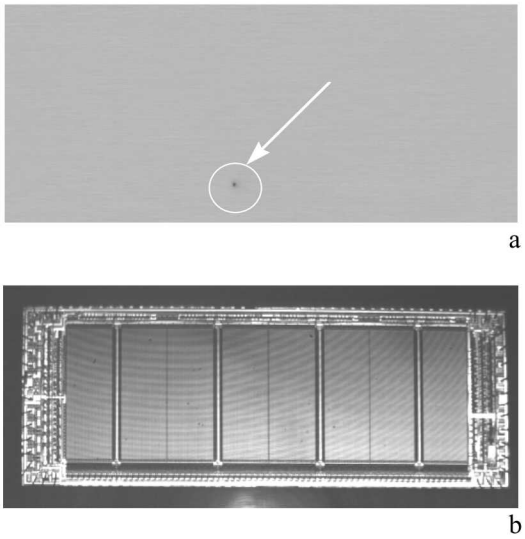

Figure 15. Entire die front side TIVA image of a 1MB SRAM showing (a) the site of a particle short. A reflected light image (b) is show of the same field of view for registration.

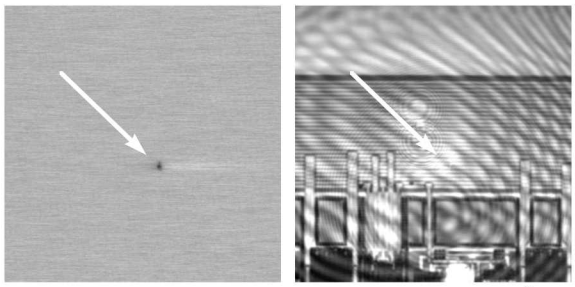

Figure 16. Backside TIVA image (a) localizing a short circuit site on a 1MB SRAM and backside reflected light (b) image of the same field of view. Note that the shorting particle on top of metal-1 is not visible from the backside in (b).

Improving Spatial Resolution

One persistent challenge with laser-based approaches to FA is spatial resolution. Using 1 μm laser wavelengths to examine 45 nm node technologies and below produces serious limits to defect localization.

Two approaches have been successfully demonstrated to improve backside spatial resolution, solid immersion lenses and substrate ultra-thinning.

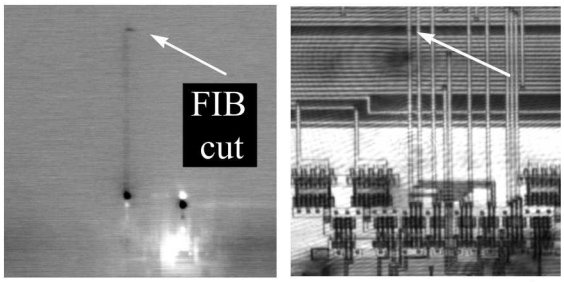

Figure 15. Backside SEI image (a) showing an open conductor resulting from an FIB cut and a reflected light image (b) for registration.

Solid Immersion Lenses (SILs)

SILs essentially increase the light collection efficiency of the optical system, increasing the numerical aperture (NA) which is inversely proportional to the spatial resolution.

The most popular SIL approach is the NAIL (NA increasing lens) [24]. An example of a NAIL is shown in Figure 16. The curvature of the NAIL lens, usually Si or GaAs, increases the NA of the optical system. The NAIL/sample interface must be very flat and clean, and the sample thickness tailored to the NAIL specifications, usually 100 µm, + 20 µm. The NAIL can be moved from location to location as needed. Figure 17 shows a TLS image on a 90 nm sample with better than 200 nm resolution using a SIL with a 1340 nm laser.

Two other SIL approaches have been described. One uses a machined hemisphere on the back of the silicon substrate to form a FOSSIL (forming substrate into SIL) [25]. A second approach uses a machined diffraction or Fresnel lens [26]. Both the FOSSIL and Fresnel approaches have no interface problems because the SIL is part of the substrate, but neither are movable like the NAIL.

More improved spatial resolution is possible using an aperture to block the central axis of the SIL. The evanescent or "darkfield" approach may produce images with resolutions approaching 70 nm with 1 µm light. [27]

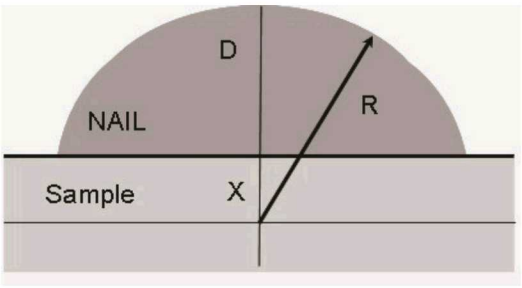

Figure 16. Schematic of a NAIL on a sample substrate

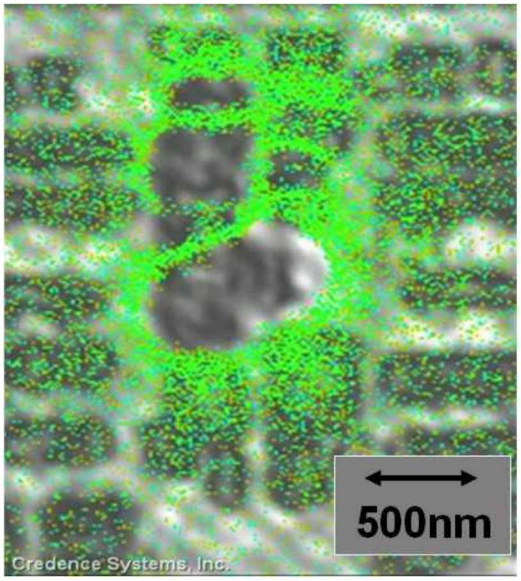

Figure 17. Example of SDL using a SIL showing better than 200 nm spatial resolution using a 1340 nm laser source. The green contrast indicates a passing condition. (Image courtesy of Steven Kasapi, Credence Systems, Inc.)

Ultra-Thinning the Silicon Substrate

Recent advances in sample preparation have enabled ultra-thinning of the silicon substrate while keeping the sample under test functional. [28] While silicon is highly absorptive and scattering to visible wavelengths, it is not complete opaque. If the silicon is thin enough, < 5 µm for example, shorter wavelength visible light can be used for active laser probing from the backside of the sample, yielding an increase in spatial resolution. SILs can also be applied to ultra-thinned samples to further improve spatial resolution, with analysis of ~ 30 nm node devices reported possible. [29]

A description of ultra-thinning techniques and results of their application are described in other sections of the Desk Reference.

Conclusion

We have described the basic physics behind active laser-based FA methods. Both localized photocurrent and thermal generation were explored through models and case studies.

Photocurrent-based (OBIC/LIVA) and TLS (OBIRCH/TIVA/SEI) methods can rapidly and precisely localize diffusion related defects and short-circuit defects and current paths. Laser methods are applicable from the front side of ICs as well as from the backside.

With proper sample preparation for optical access, laser-based FA methods can require only a few minutes to a few hours to localize defects. A better understanding of the generation physics makes it possible to gain insight into the physical nature of the located defect.

Because of their great effectiveness and future potential, photon probing methods will continue to be mainstays in IC FA for the foreseeable future and topics for development and improvement.

Acknowledgements

The authors would like to thank Romain Desplats, Phillipe Perdu, Christian Boit, Richard E. Anderson, Daniel L. Barton, Michael R. Bruce, Paiboon Tangyunyong, Jerry M. Soden, and Willian Vanderlinde for their careful review of and valuable contributions.

Sandia National Laboratories is a multimission laboratory managed and operated by National Technology & Engineering Solutions of Sandia, LLC, a wholly owned subsidiary of Honeywell International Inc., for the U.S. Department of Energy's National Nuclear Security Administration under contract DE-NA0003525.

References

1. K.S. Wills, T. Lewis, G. Billus, and H. Hoang, Optical Beam Induced Current Applications for Failure Analysis of VLSI Devices, ISTFA, 21-26, (1990).
2. E.I. Cole Jr. et al., Novel Failure Analysis Techniques Using Photon Probing with a Scanning Optical Microscope, IRPS, 388-398, (1994).
3. K. Nikawa and S. Inoue, New Capabilities of OBIRCH Method for Fault Localization and Defect Detection, Sixth Asian Test Symposium, 219-219 (1997).
4. E.I. Cole Jr. et al, Backside Localization of Open and Shorted IC Interconnections, IRPS, 129-136, (1998).
5. K. Nikawa and S. Inoue, Various Contrasts Identifiable from the Backside of a Chip by 1.3μm Laser Beam Scanning and Current Change Imaging, ISTFA, 387-392, (1996).
6. A.H. Johnston, Charge Collection in p-n junctions Excited with Pulsed Infrared Lasers, IEEE transaction on Nuclear Sciences, Vol. 40, No. 6,1694-1702, (1993).
7. T.W. Joseph, A.L. Berry, and B. Bossmann, Infrared Laser Microscopy of Structures on Heavily Doped Silicon, ISTFA, 1-7, (1992).
8. T.W. Lee, A Review of Wet Etch Formulas for Silicon Semiconductor Failure Analysis, ISTFA, 319-330, (1997).
9. P. Perdu, Comparative Study of Sample Preparation Techniques for Backside Analysis, ISTFA, 161-171, (2000).
10. Ioffe A.F., Semiconductor thermoelement and thermoelectric cooling, Inforesearch limited, (1957).
11. F. Beaudoin, X. Chauffleur, J. P. Fradin, P. Perdu, R. Desplats and D. Lewis, Modeling Thermal Laser Stimulation, Microelectronic Reliability, Vol. 41, 1477-1482, (2001).
12. Metals Handbook 8th Edition, "Vol. 1: Properties and Selection of Metals", Editor T. Lyman, American Society for Metals, Ohio, (1961).
13. G. Hass and E. Ritter, Optical Film Materials and Their Applications, Journal of Vacuum Science Technology, Vol. 4, No. 2, 71-79, (1967).
14. R. King, C.V. Schaick, and J. Lusk, Electrical Overstress of Nonencapsulated Aluminum Bond Wires, IRPS, 141-151, (1989).
15. O. Paul, M. von Arx, and H. Baltes, Process Dependent Thermophysical Properties of CMOS IC Thin Films, The 8th International Conference on Solid-State Sensors and Actuators, and Eurosensors IX, 178-181, (1995).
16. F. Beaudoin, "Localisation de Defaut par la Face Arriere des Circuits Integres", Ph.D. Thesis, Universite Bordeaux 1, No d'ordre 2605, (2002).
17. S.M. Sze, "Semiconductor Devices: Physics and Technology", John Wiely & Sons, New York, (1985).

18. C. Boit, A. Glowacki, S. Brahma, and K. Wirth, Thermal Laser Stimulation of Active Devices in Silicon – A Quantitative FET Parameter Investigation, IRPS, 357-360 (2004).
19. K. Nikawa and S. Tozaki, Novel OBIC Observation Method for Detecting Defects in Al Stripes Under Current Stressing, ISTFA, 303-310, (1993).
20. M. Palaniappan, J. M. Chin, B. Davis, M. Bruce, J. Wilcox, C. M. Chua, L. S. Koh, H. Y. Ng, S. H. Tan, J. C. H. Phang, and G. Gilfeather, New Signal Detection Methods for Thermal Beam Induced Phenomenon, ISTFA, 171-177, (2001).
21. R.A. Falk, Advanced LIVA/TIVA Techniques, ISTFA, 59-65, (2001).
22. E.I. Cole Jr. et al., Advanced Scanning Electron Microscopy Methods and Applications to Integrated Circuit Failure Analysis, Scanning Microscopy, vol. 2, no. 1, 133-150, (1988).
23. S. E. Aw, H. S. Tan, and C. K. Ong, Optical Absorption Measurements of Band-gap Shrinkage in Moderately and Heavily Doped Silicon, J. Phys.: Condens. Matter, **3,** 8213-8223, (1991).
24. S.B. Ippolito et al., High Spatial Resolution Subsurface Microscopy, Applied Physics Letters, 4071-4073, (2001).
25. T. Koyama et al., High Resolution Backside Fault Isolation Technique Using Directly Forming Si Substrate into Solid Immersion Lens, IRPS, 529-535, (2003).
26. F. Zachariasse and M. Goossens, Diffractive Lenses for High Resolution Laser Based Failure Analysis, ISTFA, 1-7, (2005).
27. P. Perdu, Failure Analysis Year in Review, IRPS Reliability Year in Review, (2010).
28. J. Beutler et al., Visible Light LVP on Ultra-Thinned Substrates, ISTFA pp. 110-114, (2014).
29. T. Eiles and P. Pardy, Visible Laser Probing (VLP) with GaP Solid Immersion Lens Demonstrating 110 nm Resolution in Common Laser Probing Applications, ISTFA pp. 39-43, (2016).